Topology optimization for hybrid additive-subtractive manufacturing

Jikai Liu[a], Albert C. To[b*]

[a]Department of Mechanical Engineering, University of Alberta, Edmonton, Canada

[b]Department of Mechanical Engineering and Materials Science, University of Pittsburgh, Pittsburgh, Pennsylvania 15261, USA

*Corresponding author. Email: albertto@pitt.edu

Abstract

Hybrid additive-subtractive manufacturing is gaining popularity by making full use of geometry complexity produced by additive manufacturing and dimensional accuracy derived from subtractive machining. Part design for this hybrid manufacturing approach has been done by trial-and-error, and no dedicated design methodology exists for this manufacturing approach. To address this issue, this work presents a topology optimization method for hybrid additive and subtractive manufacturing. To be specific, the boundary segments of the input design domain are categorized into two types: (i) Freeform boundary segments freely evolve through the casting SIMP method, and (ii) shape preserved boundary segments suppress the freeform evolvement and are composed of machining features through a feature fitting algorithm. Given the manufacturing strategy, the topology design is produced through additive manufacturing and the shape preserved boundary segments will be processed by post-machining. This novel topology optimization algorithm is developed under a unified SIMP and level set framework. The effectiveness of the algorithm is proved through a few numerical case studies.

Keywords: Topology optimization; Hybrid manufacturing; Additive manufacturing; SIMP; Level set

1. Introduction

Hybrid manufacturing indicates any combinations of two or more manufacturing methods, the principle of which is to make full use of their advantages to achieve the effect of "1+1=3" [Lauwers et al. 2014]. In this paper, hybrid manufacturing takes the specific meaning of combining additive manufacturing and subtractive machining. Specifically, additive manufacturing eliminates the geometric complexity restrictions by employing the layer-by-layer material deposition process, but the part quality is sacrificed in several aspects, e.g. poor dimensional accuracy and surface quality. As indicated by [Flynn et al. 2016], obtaining high quality part in tight tolerance is currently not feasible through additive manufacturing. In contrast, subtractive machining produces good part quality but design for subtractive machining is quite limited by the geometry complexity. Hence, these two manufacturing methods are complementary and could together form a superior manufacturing strategy, in which additive manufacturing produces the close-to-shape raw part and subtractive machining refines the raw part to achieve the desired dimensional accuracy and surface finish [Zhu et al. 2013]. It is worth noticing that, only some surfaces on a part require post-machining, e.g. surfaces come into contact with other part in an assembly.

In addition, the machining in this paper specifically means the 2.5D form feature machining, as it only requires 2.5/3-axis machines, uses less costly machine tools, cutters and clamping devices [Verma and Rajotia 2008], and requires significantly less time for code generation and rough-to-finish machining [Masmiati et al. 2012; Xu et al. 2013].

So far, the hybrid manufacturing process has been introduced and the main motivation of this paper is to explore the related topology optimization method.

Currently, topology optimization is mainly divided into three branches: SIMP (Solid Isotropic Material with Penalization) [Bendsoe and Sigmund 2004], ESO (Evolutionary Structural Optimization) [Xie and Steven 1993], and level set [Wang et al. 2003; Allaire et al. 2004]. These methods all have their unique characteristics but at the same time, are tightly associated. A few literature surveys can be found in [Eschenauer and Olhoff 2001; Rozvany 2001, 2009; Sigmund and Maute 2013; van Dijk et al. 2013; Deaton and Grandhi 2014; Munk et al. 2015].

Manufacturability issue has always been a hot topic in the topology optimization field, because the freeform topology optimization solution frequently yields non-manufacturable designs even for additive manufacturing. In the past two decades, quite a few research works have been published about manufacturing oriented topology optimization and some widely focused aspects will be briefly introduced.

Length scale control attracts the main attention for machining parts, because small voids would cause tool assess issues and thin-wall structures are hard to fabricate. Quite a few implementations are performed based on SIMP and they can be summarized into three main approaches: by adding local constraints [Poulsen 2003; Guest 2009b; Zhou et al. 2015], by applying density filters [Guest et al. 2004; Guest 2009a; Sigmund 2007, 2009; Wang et al. 2011; Schevenels et al. 2011], and by using structural skeleton-based constraints [Zhang et al. 2014]. Other than that, the length scale control can be equally realized through level set method, by employing either control functional [Chen et al. 2008b; Luo et al. 2008; Liu et al. 2015a] or constraints [Guo et al. 2014a; Xia and Shi 2015; Allaire et al. 2016; Wang et al. 2016]. An advantage of the level set method is that, the signed distance information greatly facilitates the length scale measure and control, e.g. the structural skeleton identification [Guo et al. 2014a; Xia and Shi 2015] and the contour offset [Wang et al. 2016]; and the related computation cost is not so heavy as compared to some SIMP-based implementations [Sigmund 2007]. A literature survey about the length scale control can be found in [Lazarov et al. 2016]. Injection molding/casting oriented topology optimization focuses more on the no-undercut design, because the undercuts are either non-manufacturable or requiring additional mold devices. No-undercut design has been realized through both SIMP [Zhou et al. 2002; Schramm and Zhou 2006; Stromberg 2010; Lu et al. 2012; Gersborg and Andreason 2011; Guest and Zhu 2012] and level set [Xia et al. 2010; Allaire et al. 2013] methods, which have demonstrated similar design effects. Additive manufacturing oriented topology optimization is recently very popular, and several aspects are being actively investigated including multi-material design [Gaynor et al. 2014; Meisel and Williams 2015], the buildability issue [Bracket et al. 2011; Leary et al. 2014], the material anisotropy [Liu et al. 2016], and the design interpretation [Zegard and Paulino 2015]., etc. Majority of these aspects are still not well addressed [Bracket et al. 2011; Meisel and Williams 2015], and a large number of related publications can be foreseen in the near future.

In summary, to the best of the authors' knowledge, topology optimization for hybrid manufacturing has not been addressed despite an urgent need for such method.

A schematic plot of the topology optimization for hybrid manufacturing is demonstrated in Fig. 1. Note that side faces of the cube are fitted with 2.5D machining features, while the top and bottom faces employ the freeform evolvement because there is no stringent quality requirement. The pure 2.5D machining feature-based result is also demonstrated for reference.

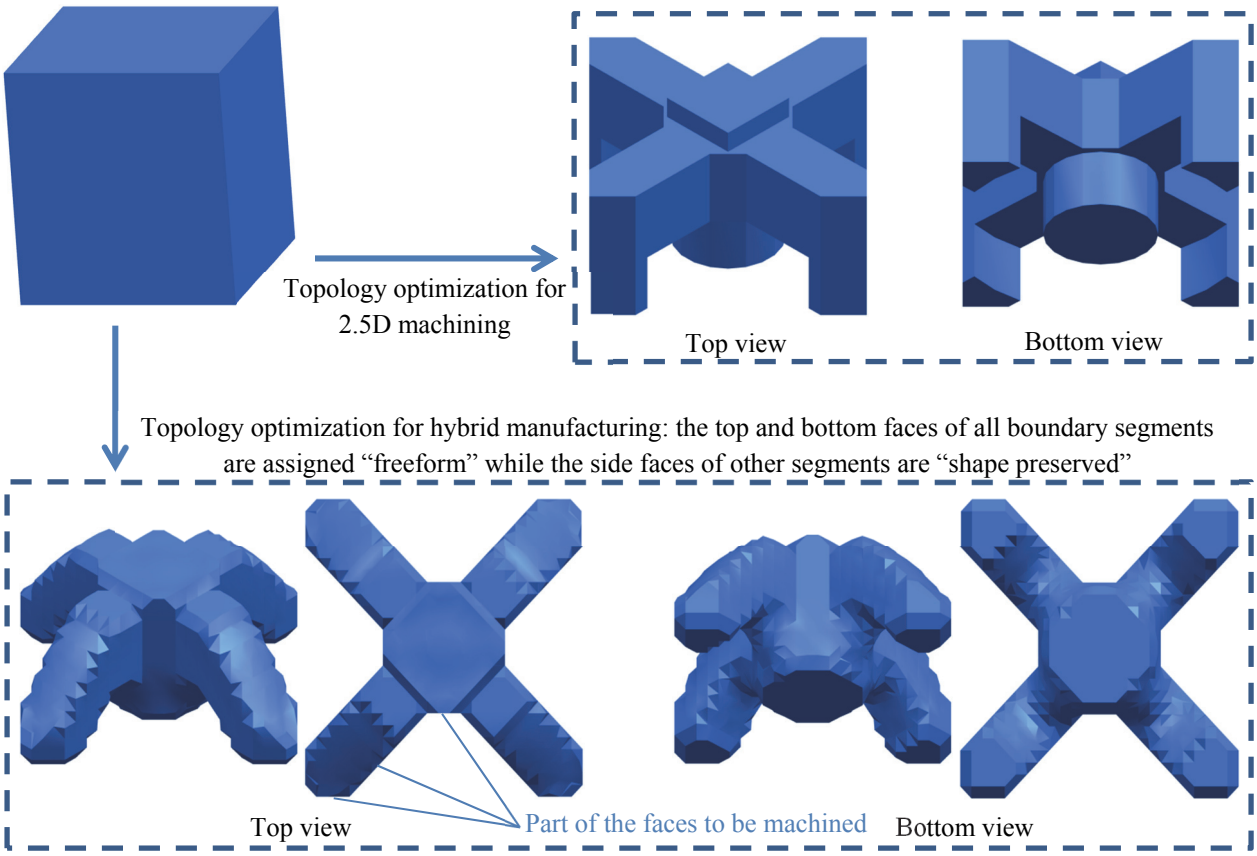

Fig. 1 Comparison of the optimal designs obtained through (top right panel) 2.5D machining feature-based optimization and (bottom panel) by the proposed optimization method for hybrid manufacturing, respectively

It is worth noticing that, this topology optimization method for hybrid manufacturing is built on our previously developed 2.5D machining feature-based level set method [Liu and Ma 2015], where similar procedures are employed. On the other hand, the implementation under the density-based framework is technically more challenging: (i) it is non-trivial to identify the structural boundary based on the blurred density field and accordingly perform the structural boundary-based feature fitting; and (ii) feature-based sizing/shape optimization is not supported under the density-based framework and the feature fitting has to be repeatedly performed to update the feature profiles, which causes convergence difficulties. In summary, both the implementation details and numerical characteristics are very different from the previous level set based implementation. The challenges are technically solved in this work and more specifications will be presented in later sections.

2. Literature survey and research motivation

2.1 Geometric feature-based topology optimization

Machining feature conventionally is an important concept in computer-aided design (CAD)/computer-aided manufacturing (CAM) system. It is defined on the geometric feature that can be machined in a single operation and is attached with abundant machining information, including the required cutting methods, tools, suggested tolerances, surface finish specifications, and estimated manufacturing cost, etc. [Hoque et al. 2013]. Functionally, machining feature-based design supports seamless CAD/CAM

integration and automated computer-aided process planning (CAPP). Among the machining feature types, 2.5D machining features are greatly preferred and widely accepted by the manufacturing community because the related manufacturing time and cost are much lower compared to the 3D freeform features. From this pespective, it would be beneficial if topology optimization methods could produce 2.5D machining feature-based design solutions instead of only 3D freeform results. Therefore, this sub-section reviews existing geometric feature-based topology optimization methods, which have the potential to be further developed to support the 2.5D machining feature-based design.

The implementations based on the SIMP method can be categorized into two branches: through the multi-component movement or through the geometric feature projection.

For multi-component movement, a review can be found in [Zhang et al. 2011], and the main idea is to concurrently optimize the components' position parameters through a finite difference based sensitivity analysis and the support structure through the SIMP method. A finite circle method was developed to avoid the component overlap. However, the interface areas between the components and the support structure were repeatedly re-meshed and the adopted finite difference method required multi-time finite element analyses in each optimization loop, both of which reduced the overall computational efficiency. Later, some improvements were achieved by adopting the level set-based geometric feature representation and the X-FEM [Zhang et al. 2012; Kang and Wang 2013; Xia et al. 2013], which altogether eliminates the repeated re-meshing and the in-loop multi-time finite element analyses. Zhang et al. [2015a] also performed the multi-component design based on the combined SIMP and level set representations and they proposed a structural skeleton-based non-overlap constraint. Kang et al. [2016] performed the multi-component design completely under the level set framework, where the level set-based distance constraint is proposed to prevent the multi-component overlap. Recently, the rivet or bolt connections were addressed in [Zhu et al. 2015; Gao et al. 2015].

For geometric feature projection, Ha and Guest [2014] and Guest [2015] employed the Heaviside projection to solve the geometric feature layout problems, which enabled the creation of small circular features and realized the non-overlap control. Recently, Norato et al. [2015] inherited the idea from [Guo et al. 2014b] by filling the design domain completely with geometric features and the related freedoms were optimized through a proposed geometry projection method.

The implementations under the level set framework can be traced back to Chen et al. [2007; 2008a]. They performed the concurrent geometric feature layout and support structure optimization under a unified level set framework. Both parametric and discrete level set representations were employed and combined through R-functions. Cheng et al. [2006] and Mei et al. [2008] also employed the parametric level set function for geometric feature modeling and optimization. More importantly, they calculated the topological derivative to insert geometric features during the early optimization loops, which enabled the geometric feature-based design from an arbitrary input. Gopalakrishn and Suresh [2008] contributed the feature-specific topological derivative algorithm introducing both internal and boundary features under the 2D scheme. This work provided a good theoretical basis for topological sensitivity analysis on inserting certain geometric features. Zhou and Wang [2013] manipulated the geometric features in a different manner. They regulated the boundary velocity fields of the geometric features via least squares fitting in order to reserve their shape characteristics; then, through the standard Hamilton Jacobi equation based design update, they accomplished the concurrent geometric feature control and freeform support structure optimization under a unified discrete level set framework. This least squares fitting idea was exploited by Liu and Ma [2015] to enable the geometric feature insertion to produce 2.5D machining

feature-based topology design. Recently, Guo et al. [2014b] and Zhang et al. [2016] contributed a novel level set method by arbitrarily distributing geometric features inside the design domain. By optimizing the related freedoms, the purely geometric feature-based topology design could be derived.

All the methods reviewed above, developed under the SIMP/level set framework, have realized the purely geometric feature-based design or the combined geometric feature layout and support structure design, in which the geometric features can be either solid or void and have the freedom of movement, scaling and rotation. However, there are still gaps to be addressed in order to make these methods support the 2.5D machining feature-based topology design, because they are not initiated for this purpose and the machining rules are frequently violated. For instance, subtractive machining removes materials from the boundary towards inside; however, many of the methods could generate interior void features which are non-manufacturable. For the exception, the method proposed in [Liu and Ma 2015] was customized for 2.5D machining feature-based topology design. The generated results are quite friendly to 2.5D machining. It meets the scope of this paper to design parts manufactured through 'hybrid additive manufacturing and 2.5D machining'. Hence, it will be used as the basis of this paper to develop the topology optimization method for hybrid manufacturing.

2.2 Topology optimization for additive manufacturing

Additive manufacturing removes the complexity restrictions of the traditional manufacturing methods and has made structural topology design much more creative than before. For instance, a direct benefit is that the intermediate densities can now be mapped into 3D printing units and several researches have proved its feasibility through real testing [Khanoki and Pasini 2012; Tang et al. 2015; Zhang et al. 2015b].

On the other hand, new rules and constraints are introduced as well and there is a lack of solutions for topology optimization for additive manufacturing as pointed out in [Bracket et al. 2011; Meisel and Williams 2015]. Therefore, there are increasingly more publications targeting this area and several problems have been addressed even though not fully solved, including the non-support design [Bracket et al. 2011; Leary et al. 2014; Garden and Schneider 2015], the multi-material design [Gaynor et al. 2014], the no-interior void design [Liu et al. 2015b], the build direction design [Ulu et al. 2015], and the topology design interpretation for additive manufacturing [Zegard and Paulino 2015].

As summarized above, topology optimization for hybrid additive and subtractive manufacturing is a new topic which will be addressed in this work.

3. Simplified density representation

In [Gersborg and Andreasen 2011], a simplified density representation was developed to satisfy the casting constraint of no interior void and undercut. Because of the similarities between 2.5D machining and casting, the simplified density representation is also applicable to the 2.5D machining part design through certain tailoring. Therefore, the simplified density representation is briefly introduced in this section.

In contrast to the conventional density representation, the simplified approach reduces the design space by assigning two density variables to each row or column of elements, see Fig.2.

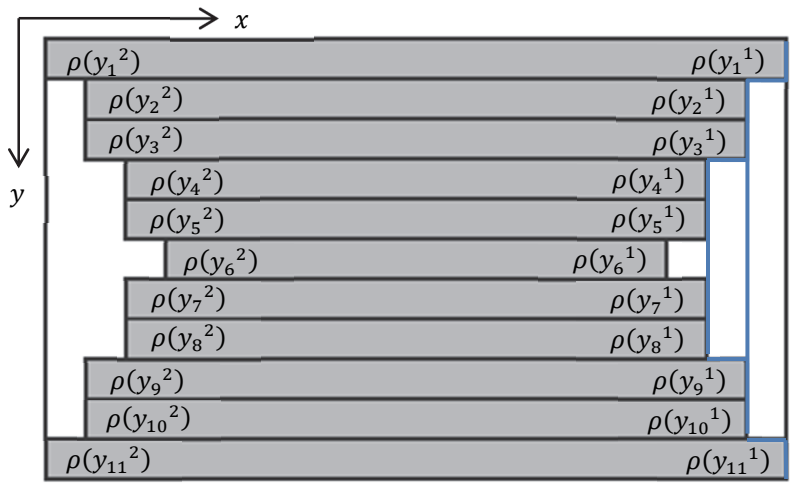

Fig. 2 Row density variables

Then, the following procedures are applied to project the row density variables to the entire density field and the same procedure is applied to column density variables.

(1) Normalize the x-coordinate:

$$s_i = x_i / L_x \tag{1}$$

in which x_i is the center x-coordinate of the element i and L_x is the length of the row.

(2) Stretch the simplified density variable:

$$\hat{\rho}(y_j^k) = (a+b)\rho(y_j^k) - b, \qquad 0 < b < a, \qquad \hat{\rho}(y_j^k) \in [-b, a] \tag{2}$$

Initially, $\rho(y_j^k) \in [0,1]$ for the kth row density vairble of the jth row, and purpose of the stretching is to enable the boundary elements approaching solid or void when performing the approximate Heaviside projection, see Fig. 3. The positive constants a and b represent the stretched amounts in the lower and upper bounds, respectively.

(3) Calculate the element densities through Heaviside projection:

$$\begin{aligned} \tilde{\rho}^1(x_i, y_j) &= H(s_i, \hat{\rho}(y_j^1); \beta) \\ \tilde{\rho}^2(x_i, y_j) &= 1 - H(s_i, \hat{\rho}(y_j^2); \beta) \\ \tilde{\rho} &= \tilde{\rho}^1 + (1 - \tilde{\rho}^1)\tilde{\rho}^2 \end{aligned} \tag{3}$$

in which $\tilde{\rho}(x_i, y_j)$ is the projected element density. $H(s_i, \hat{\rho}(y_j^k); \beta)$ is the approximate Heaviside projection, which is defined in Eq. (4) [Liu et al. 2015b]. $\beta > 0$ controls the steepness of the approximation.

$$H(s, \rho; \beta) = \frac{e^{\beta(\rho - s)}}{1 + e^{\beta(\rho - s)}} \tag{4}$$

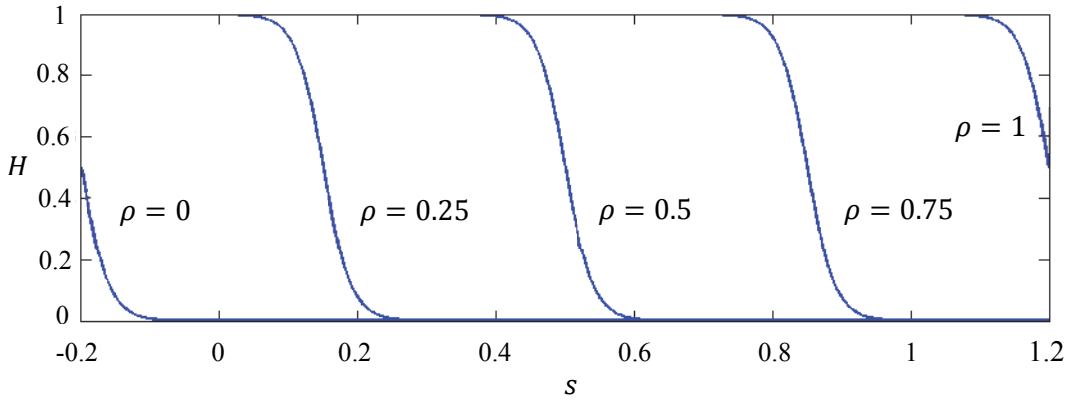

Fig. 3 Schematic plot of the approximate Heaviside projection ($\beta = 50$, $a = b = 0.2$)

Then, the general compliance minimization problem is constructed as:

$$\begin{aligned} min.\ \ & C = \sum \boldsymbol{u}^T \tilde{\rho}(x_i, y_j)^p \boldsymbol{k}\boldsymbol{u} \\ s.t.\ \ & g = \sum \tilde{\rho}(x_i, y_j) v - V_{max} \le 0 \\ & \boldsymbol{K}(\tilde{\rho})\boldsymbol{U} = \boldsymbol{F} \\ & 0 < \rho_{min} \le \tilde{\rho}(x_i, y_j) \le 1 \end{aligned} \tag{5}$$

where $\boldsymbol{U}$ and $\boldsymbol{F}$ are the global displacement vector and loading vector, respectively. $\boldsymbol{K}$ is the global stiffness tensor. $\boldsymbol{u}$ is the element displacement vector, $\boldsymbol{k}$ is the element stiffness tensor, and v is the material volume of a solid element. ρ_{min} is the lower bound of the element density and V_{max} is the upper bound of the total material volume.

Solution of this problem is simple and the sensitivity results are derived as [Bendsoe and Sigmund 2004]:

$$\frac{\partial C}{\partial \tilde{\rho}(x_i, y_j)} = -\boldsymbol{u}^T p \tilde{\rho}(x_i, y_j)^{p-1} \boldsymbol{k}\boldsymbol{u}, \quad \frac{\partial C}{\partial \rho(y_j{}^k)} = \sum_i \frac{\partial C}{\partial \tilde{\rho}(x_i, y_j)} \frac{\partial \tilde{\rho}(x_i, y_j)}{\partial \rho(y_j{}^k)} \tag{6}$$

and for the volume constraint, Eq. (7) is derived.

$$\frac{\partial g}{\partial \tilde{\rho}(x_i, y_j)} = v, \quad \frac{\partial g}{\partial \rho(y_j{}^k)} = \sum_i \frac{\partial g}{\partial \tilde{\rho}(x_i, y_j)} \frac{\partial \tilde{\rho}(x_i, y_j)}{\partial \rho(y_j{}^k)} \tag{7}$$

4. 2.5D machining feature generation

According to the row/column density variables, the material growth and elimination both happen at the structural boundary, which makes it similar to the velocity field concept in level set method [Wang et al. 2003; Zhou and Wang 2013]. Therefore, the 2.5D machining feature-based level set method [Liu and Ma 2015] can be re-developed under the density-based framework. As depicted in Fig. 2, the blue colored contour is an approximation of the 0/1 interface which is a compound slot feature manufacturable through 2.5D machining. This implementation will be meaningful because as widely recognized; density-based method employs the advantages of easy implementation and good robustness, and thus is widely adopted by commercial codes. There are several reasons for level set method not appearing in commercial codes;

for example, it lacks stability as so many tuning parameters are required and it is difficult to solve problems with many constraints under the non-parameterized formulation.

In order to realize the 2.5D machining feature-based design, feature generation is critical but it has not been realized by most feature-based topology optimization methods. Some feature generation techniques such as feature-specific topological derivative [Cheng et al. 2006; Mei et al. 2008; Gopalakrishn and Suresh 2008] would not work under the density-based framework. Therefore, the feature fitting algorithm developed by Liu and Ma [2015] is reused here and some adaptions will be made according to the characteristics of the density-based method.

The primary adaption is that the previously defined three steps are now expanded into four: define the feature library, make segmentation, solve the least squares fitting problem, and re-distribute the element densities.

4.1 Feature library construction

Even though density-based method will be utilized in this work, the level set functions are still employed to represent the machining features. The level set functions are able to greatly facilitate the boundary segmentation, the solution of the least squares fitting problem, and also the element density redistribution. In fact, the hybrid application of density-based and level set methods is quite popular these days [Kang and Wang 2013; Xia et al. 2013; Zhang et al. 2015a] and is advocated by many respected researchers [Sigmund and Maute 2013].

Briefly revisiting the level set-based feature representation, a square feature (see Fig. 4) is represented by:

$$\Phi_f(\boldsymbol{X}) = min\{\frac{H_s}{2} - (x - x_0), \frac{H_s}{2} + (x - x_0), \frac{H_s}{2} - (y - y_0), \frac{H_s}{2} + (y - y_0)\} \tag{8}$$

in which (x_0, y_0) is the feature primitive center coordinates and H_s is the square length.

Then, a complex geometry can be constructed through Boolean operations of the individual feature primitives as:

$$\begin{aligned} \Phi_{f1} \cup \Phi_{f2} &= max\left(\Phi_{f1}, \Phi_{f2}\right) \\ \Phi_{f1} \cap \Phi_{f2} &= min\left(\Phi_{f1}, \Phi_{f2}\right) \\ \Phi_{f1} \setminus \Phi_{f2} &= min\left(\Phi_{f1}, -\Phi_{f2}\right) \end{aligned} \tag{9}$$

In addition, the machining features are distinguished into two types: the front machining feature and the side machining feature; see Fig. 4. The former is applied in case that the mounting boundary segment is perpendicular to the cutter axis and the latter is employed in case that the mounting boundary segment is parallel to the cutter axis. A general 2.5D machining feature library is presented in Fig. 5 for reference.

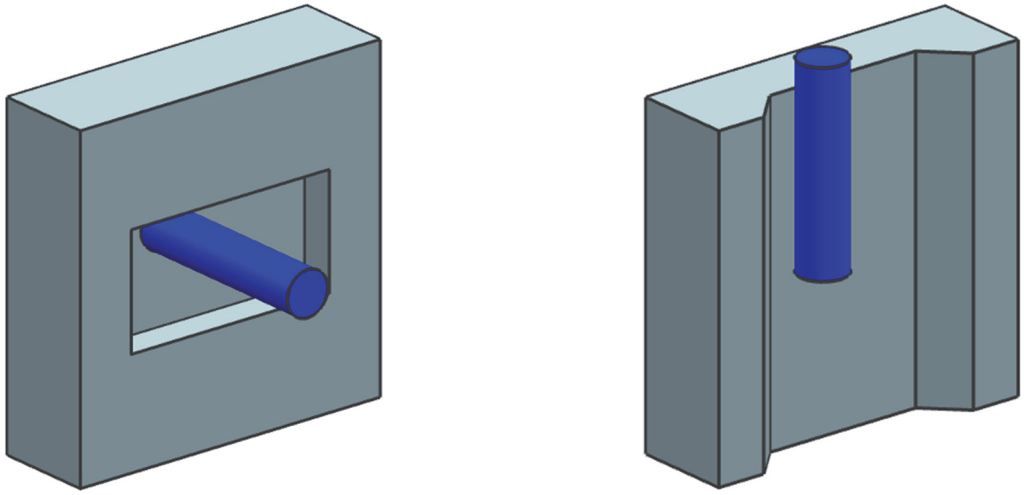

(a) Front machining feature (b) Side machining feature

Fig. 4 Definition of front and side machining features (the dark blue color represents the cutter)

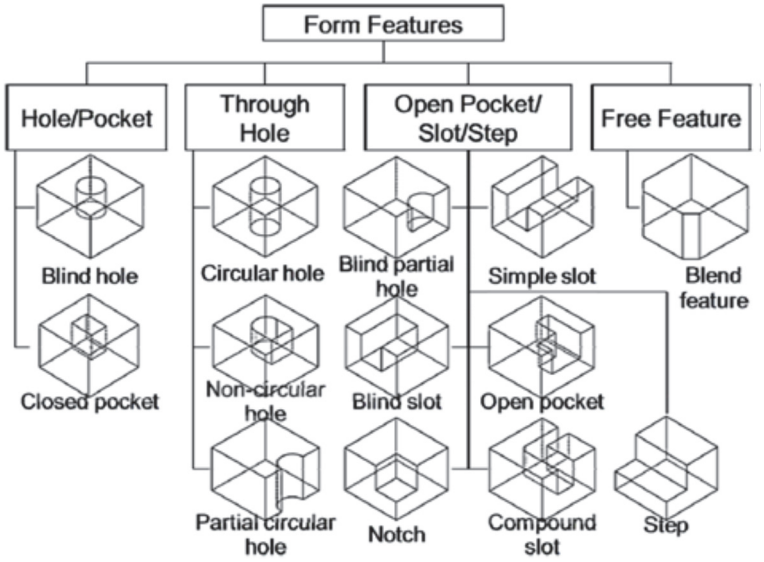

Fig. 5 2.5D machining feature classification [Kang et al. 2014]

It is noted that the candidate feature types will be specified for each case study in later sections.

4.2 Boundary segmentation

Boundary segmentation is assisted by the level set-based feature representation. For instance, in Fig. 6a, the initial design domain and its top edge are represented by:

$$\Phi(\boldsymbol{X}) = \Phi_0(\boldsymbol{X}) = min\{\frac{L_0}{2} - (x - x_0), \frac{L_0}{2} + (x - x_0), \frac{H_0}{2} - (y - y_0), \frac{H_0}{2} + (y - y_0)\}$$
$$\frac{H_0}{2} - (y - y_0) = 0, \quad (top\ edge\ 0\ for\ feature\ insertion) \tag{10}$$

If one slot feature is fitted from the top edge, as depicted in Fig. 6b, the updated level set function will be:

$$\Phi(\boldsymbol{X}) = \Phi_0(\boldsymbol{X}) / \Phi_1(\boldsymbol{X}) \tag{11}$$

$$\Phi_1(\boldsymbol{X}) = min\{\frac{L_1}{2} - (x - x_1), \frac{L_1}{2} + (x - x_1), \frac{H_1}{2} - (y - y_1), \frac{H_1}{2} + (y - y_1)\}$$

$$y_1 = y_0 + \frac{H_0}{2} - \frac{H_1}{2}, \quad (mounting\ relationship)$$

$$\frac{H_1}{2} + (y - y_1) = 0, \quad (top\ edge\ 1\ for\ feature\ insertion)$$

In Eq. (11), there are two points to be noticed: the slot feature is inserted from the top edge 0 in the *y* direction and therefore, its center *y*-coordinate is calculated based on the mounting relationship; in addition, a new top edge 1 is generated after a feature has been inserted and will be used to generate new slot features; see Fig. 6c.

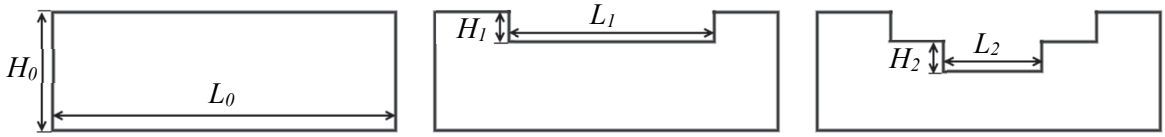

(a) (b) (c)

Fig. 6 Procedural boundary segmentation

4.3 Least squares problem

The least squares fitting problem is constructed by comparing the density fields and specifically can be expressed as:

$$min.\ J = \sum \left(H\left(\Phi(x_i, y_j, \boldsymbol{s})\right) - \tilde{\rho}(x_i, y_j) \right)^2 \tag{12}$$

By solving this problem, the best-fit feature parameter set to be inserted can be derived. If there are multiple feature candidates, it will go through an outer loop to determine the best-fit feature type.

On the other hand, the material volume cannot be kept constant through solution of Eq. (12) and occasionally, there could be big fluctuations. This inconsistency will lead to numerical instability and negatively impact the optimality. Hence, in order to preserve the volume, a volume-preserving functional is proposed and integrated into the least squares fitting problem, which is changed into:

$$min.\ J = \sum \left(H\left(\Phi(x_i, y_j, \boldsymbol{s})\right) - \tilde{\rho}(x_i, y_j) \right)^2 + w \cdot abs\left\{ \sum H\left(\Phi(x_i, y_j, \boldsymbol{s})\right) - \sum \tilde{\rho}(x_i, y_j) \right\} \tag{13}$$

for feature fitting in *x* direction; and:

$$min.\ J = \sum \left(H\left(\Phi(x_i, y_j, \boldsymbol{s})\right) - \bar{\rho}(x_i, y_j) \right)^2 + w \cdot abs\left\{ \sum H\left(\Phi(x_i, y_j, \boldsymbol{s})\right) - \sum \bar{\rho}(x_i, y_j) \right\} \tag{14}$$

for feature fitting in *y* direction.

In Eq. (13) and (14), w is a weight factor which controls the volume-preserving effect. If it is big enough, the volume-preserving requirement can be well satisfied.

4.4 Element density re-distribution

Once the best-fit feature type and its parameter set are determined, the row/column density variables need to be recalculated, which is trivial in implementation. Then, the element densities are being redistributed as well, following the approximate Heaviside projection as illustrated in the last section.

5. Optimization algorithm

Based on the density-based optimization and adapted feature fitting algorithm, the overall flow chart of the proposed optimization algorithm is illustrated in Fig. 7.

About the flow chart, there are a few points to be noted:

(1) The boundary segments are distinguished into two types based on the design intent: the shape preserved boundary segments which will be post machined and the freeform boundary segments which is purely additive manufactured. The former will be fitted with 2.5D machining features while the latter employs the freeform boundary evolvement. In addition, certain boundary segments can be predefined as non-designable and the related row/column density variables will just be fixed.

(2) IterNum is short for the iteration number and *N* is a predefined value which determines the frequency of feature fitting. In other words, new feature generation and the existing feature update are performed once for every *N* iterations.

(3) Scale control is an important issue related to the feature generation, because too many feature primitives will complicate the geometry manipulation and reduce the manufacturability. Hence, two approaches have been proposed for scale control. The first approach is to predefine a threshold value L_{lim} so that only boundary segments of size larger than L_{lim} will be considered for feature fitting; see Fig. 7. The other approach is to predefine the layers of feature fitting.

(4) The volume constraint is addressed through the Augmented Lagrange method which employs the Lagrange multiplier as:

$$\lambda_{k+1} = \lambda_k + \mu_k\left(\int_D H(\Phi)d\Omega - V_{max}\right)$$
$$\mu_{k+1} = \alpha\mu_k \ \ where\ 0 < \alpha < 1 \tag{15}$$

in which μ is the penalization factor and α is its adjustment parameter.

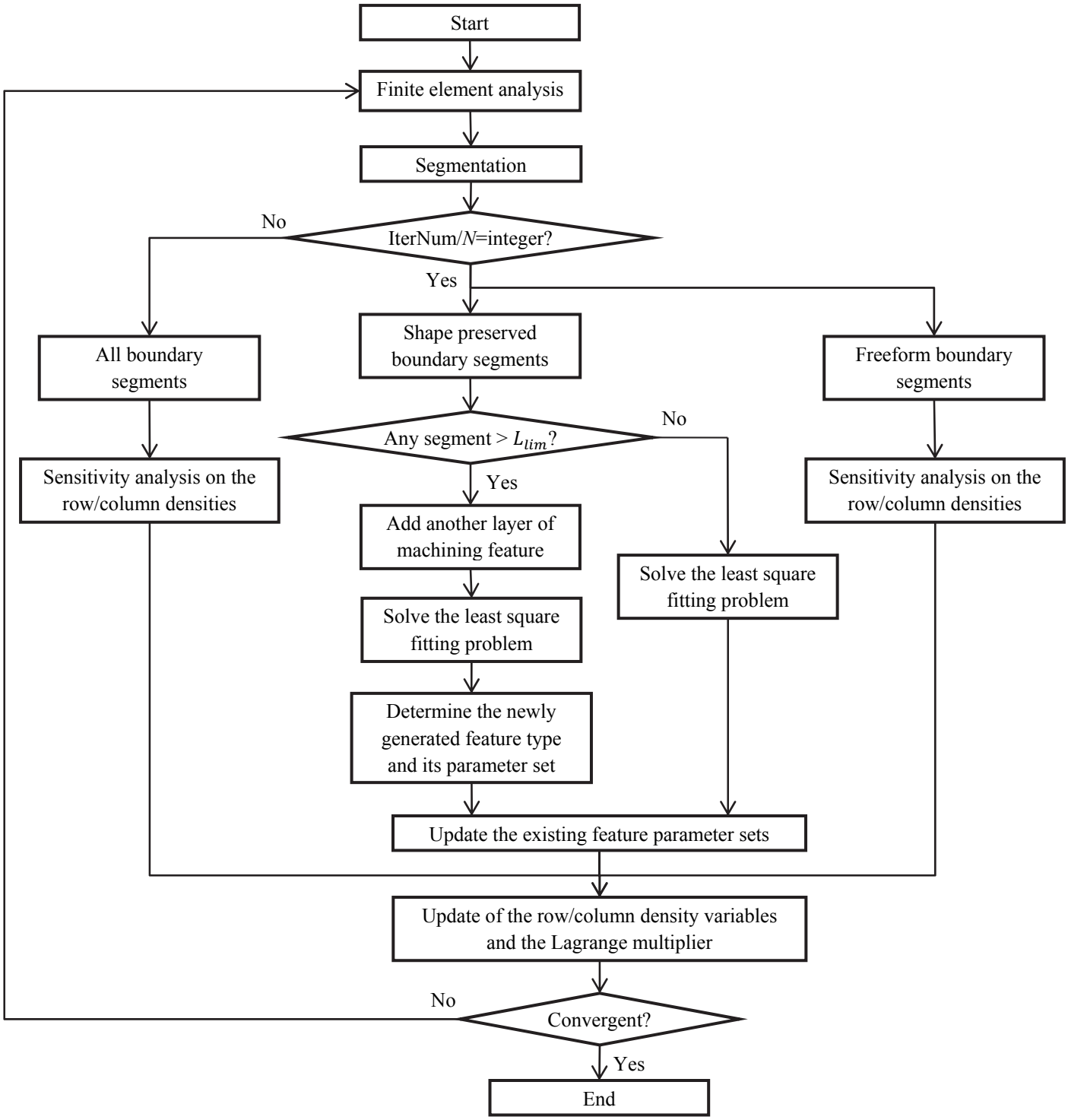

Fig. 7 Overall flow chart of the proposed optimization algorithm

6. Implementation and numerical considerations

6.1 2D examples

This sub-section presents two 2D numerical examples in order to validate the proposed optimization algorithm. For the first problem, the boundary condition is demonstrated in Fig. 8a and the optimization problem is to minimize the structural compliance constrained by the maximum material volume ratio of 0.3. For the cantilever structure problem, the boundary condition is plotted in Fig. 9a and the optimization problem is to minimize the structural compliance under the material volume ratio constraint of 0.6. For both examples, the candidate slot feature presented in Fig. 8b is applied. Only row density variables are considered and therefore, only the side edges will be applied for feature fitting while the top and bottom edges are non-designable. In addition, the predefined one-layer, two-layer, and three-layer feature fitting are studied, respectively. The optimization results are demonstrated in Fig. 8(c-f) and Fig. 9(b-d).

(a) Design domain and boundary condition

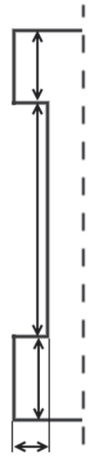

(b) Candidate slot feature

(c) Freeform design without feature fitting

(d) Forced one-layer feature fitting

(e) Forced two-layer feature fitting

(f) Forced three-layer feature fitting

Fig. 8 Foot-supported beam problem

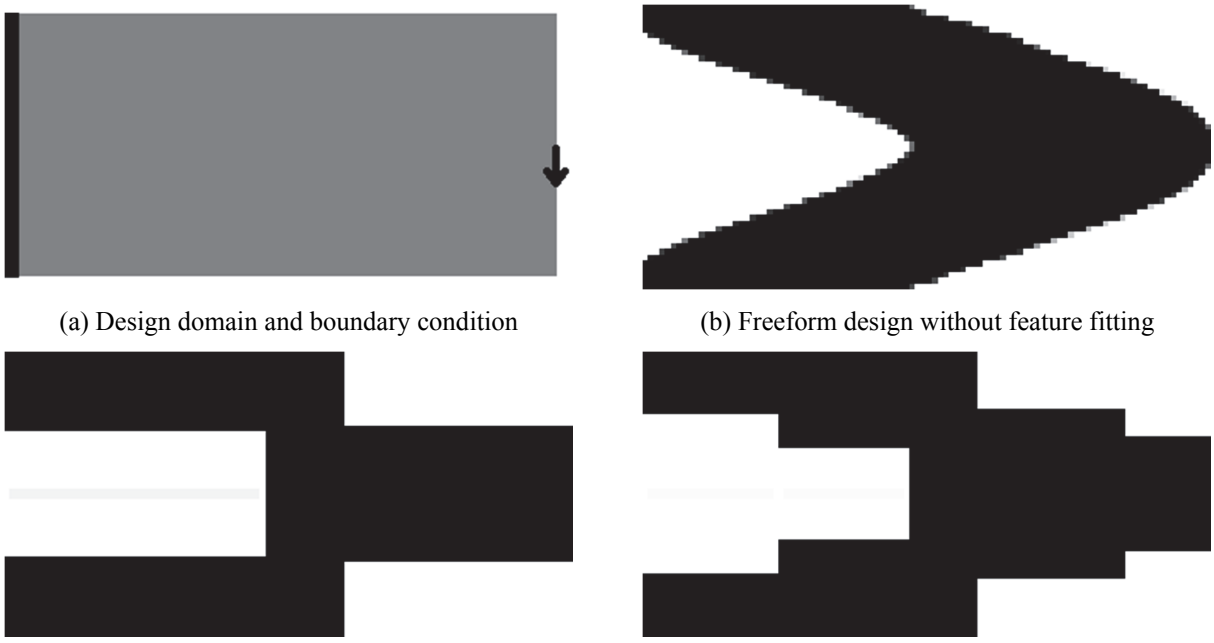

(a) Design domain and boundary condition

(b) Freeform design without feature fitting

(c) Forced one-layer feature fitting

(d) Forced two-layer feature fitting

Fig. 9 Cantilever structure problem

Conclusions can be drawn from the two examples that, the proposed optimization algorithm is effective and the feature-based results could approach the freeform design in overall material layout by increasing the layers of feature fitting.

6.2 Multi-directional density variables

This subsection explores the concurrent application of the row/column density variables. Previously in [Lu and Chen 2012], the multi-directional machining/casting constraints were developed to realize the multi-directional material removal; see Fig. 10 for an example. However, there could be a large number of constraints to be addressed and a growth interface is required which would restrict the design flexibility. Hence, the row/column density variables are still preferred for multi-directional problems.

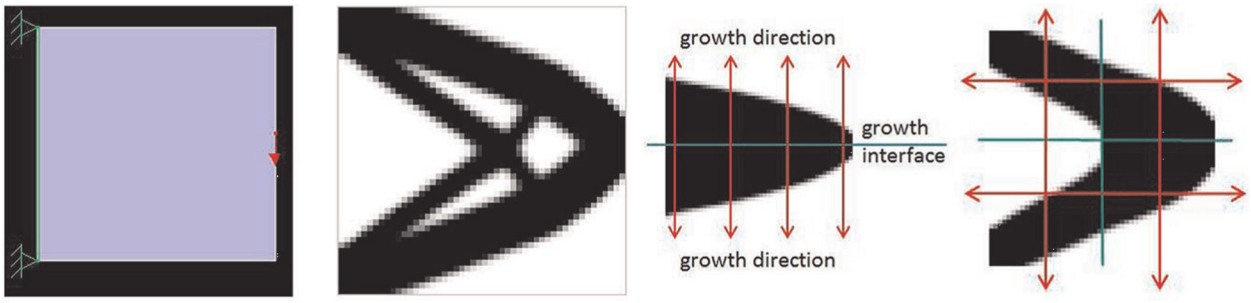

(a) Boundary condition

(b) Optimization without constraint

(c) Optimization with two-directional constraint

(d) Optimization with four-directional constraint

Fig. 10 Topology optimization with multi-directional constraints [Lu and Chen 2012]

Inspired by the R-functions adopted by level set geometry representation [Chen et al. 2007, 2008a], the same technique can be applied to combine the row and column density projections. Equations (16) and (17) presents the Heaviside projections based on the row and column density variables, respectively.

$$\begin{cases} \tilde{\rho}^1(x_i, y_j) = H(s_i, \hat{\rho}(y_j{}^1); \beta) \\ \tilde{\rho}^2(x_i, y_j) = 1 - H(s_i, \hat{\rho}(y_j{}^2); \beta) \\ \tilde{\rho} = \tilde{\rho}^1 + (1 - \tilde{\rho}^1)\tilde{\rho}^2 \end{cases} \quad (Heaviside\ projection\ of\ the\ row\ density\ varibles) \tag{16}$$

$$\begin{cases} \bar{\rho}^1(x_i, y_j) = H(s_j, \hat{\rho}(x_i{}^1); \beta) \\ \bar{\rho}^2(x_i, y_j) = 1 - H(s_j, \hat{\rho}(x_i{}^2); \beta) \\ \bar{\rho} = \bar{\rho}^1 + (1 - \bar{\rho}^1)\bar{\rho}^2 \end{cases} \quad (Heaviside\ projection\ of\ the\ column\ density\ varibles) \tag{17}$$

Then, the real element densities can be calculated by intersecting the separately projected density fields, as:

$$\tilde{\rho} \cap \bar{\rho} = min(\tilde{\rho}, \bar{\rho}) \tag{18}$$

To prove its effectiveness, the foot-supported beam is studied again and the optimization result is demonstrated in Fig. 11.

Fig. 11 Topology optimization with multidirectional density variables

6.3 Topology optimization for hybrid manufacturing

Once the multi-directional density variables can be concurrently applied, the proposed topology optimization algorithm for hybrid manufacturing can be fully implemented.

The 2D foot-supported beam example is repeated by assigning the side edges to be shape preserved and the top and bottom edges to be freeform. Influence of the feature fitting interval N is explored by assigning the values of 16, 18, 20, 22, and 24, respectively. The related optimization results are presented in Fig. 12. It can be observed from Fig. 12 that the algorithm effectively converges regardless of the feature fitting interval N. The optimized structural compliances are very close even though these results are not totally identical. Hence, it implies that the optimality of the proposed algorithm is only loosely associated with the feature fitting interval selection.

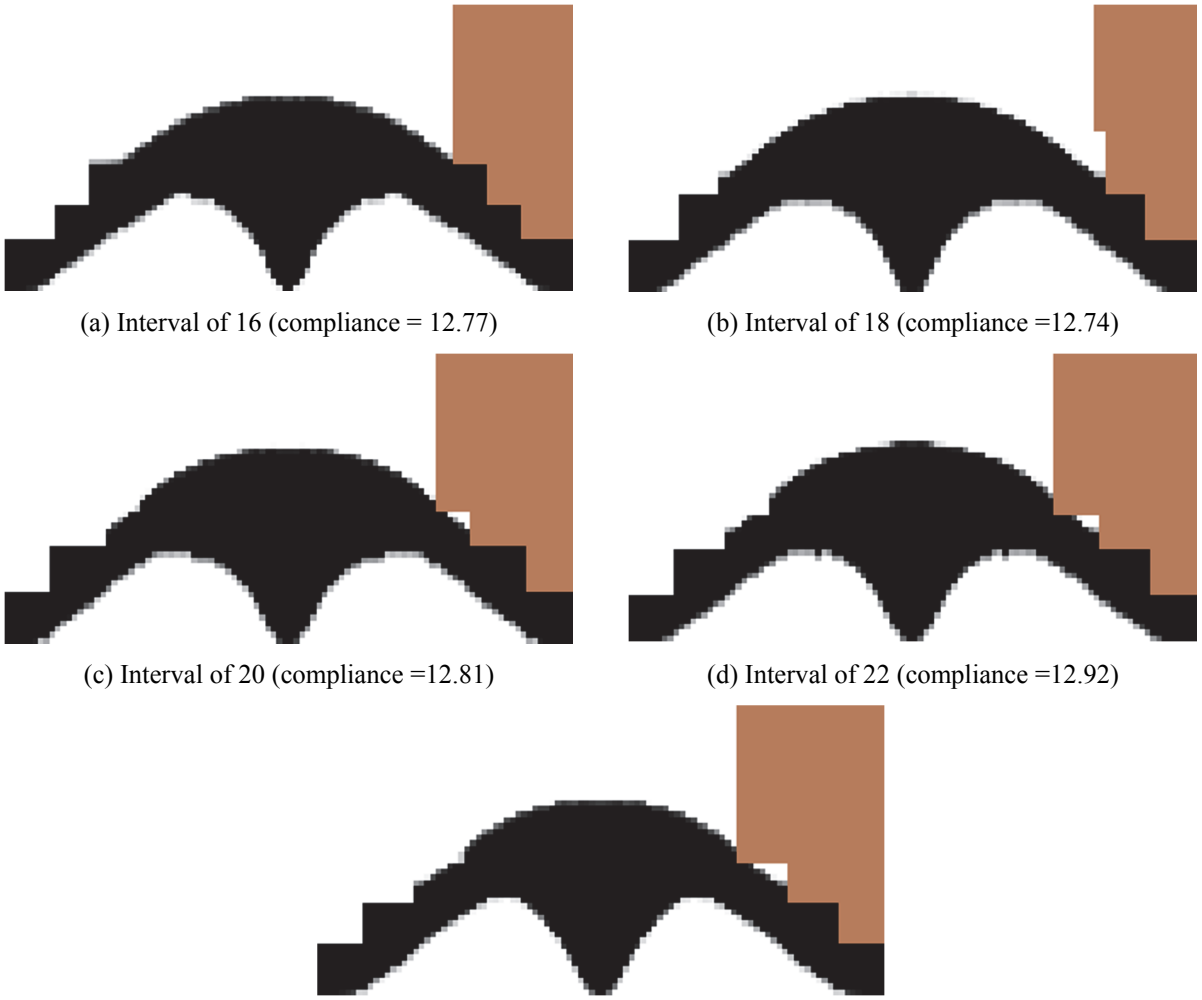

(a) Interval of 16 (compliance = 12.77)

(b) Interval of 18 (compliance =12.74)

(c) Interval of 20 (compliance =12.81)

(d) Interval of 22 (compliance =12.92)

(e) Interval of 24 (compliance =12.68)

Fig. 12 Topology optimization for hybrid manufacturing with different feature fitting intervals (the grey color represents the three-layer compound machining feature fitted from the right face)

7. 3D examples

In this section, a few 3D examples will be studied to prove the effectiveness of the topology optimization method for hybrid manufacturing.

7.1 Cube structure problem

First, the cube structure problem is studied, of which the initial design domain (24*24*15) and the attached boundary conditions are presented in Fig. 13. A force of magnitude 2 is loaded at the bottom center and the four bottom corners shown in dark blue color are fixed. The solid material employs a Young's modulus value of 1 and Poison's ratio value of 0.3. The optimization problem is to minimize the structural compliance under the maximum material volume ratio of 0.3. Given the surface categorization, the four side faces are shape preserved while the top and bottom ones are freeform. The side machining feature candidate presented in Fig. 13b is employed because the cutter axis is assumed to be perpendicular to the top and bottom surfaces.

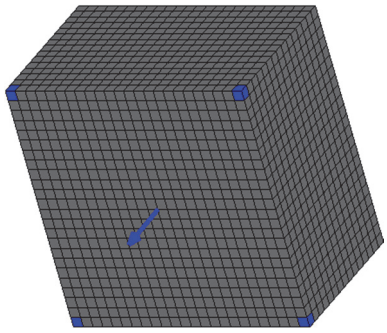

(a) Boundary condition in the bottom view

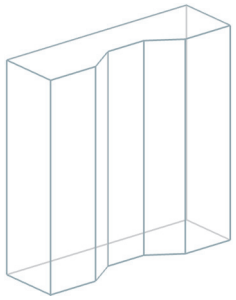

(b) Side machining feature candidate

Fig. 13 Problem setup

Two schemes will be explored in this example with the threshold value L_{lim} equal to 24*15 and 0.5*24*15, respectively. Correspondingly, the optimization results are demonstrated in Fig. 14.

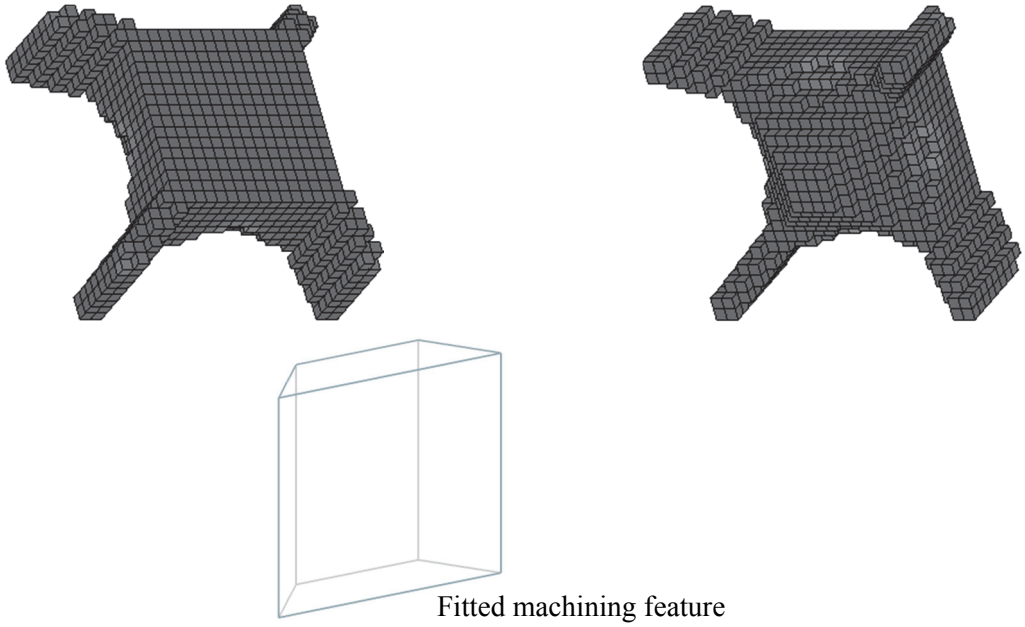

Fitted machining feature

(a) Result with $L_{lim} = 24 * 15$ (compliance = 15.19)

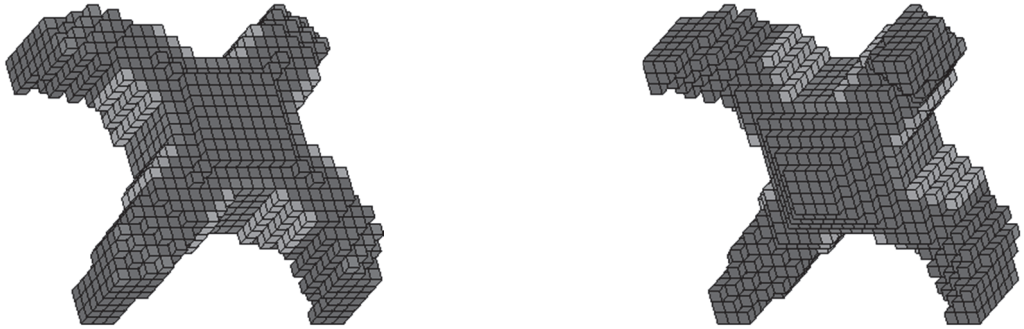

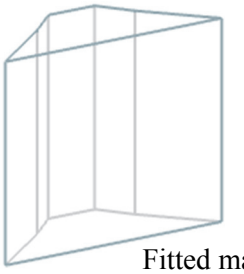

Fitted machining feature

(b) Result with $L_{lim} = 0.5 * 24 * 15$ (compliance = 14.60)

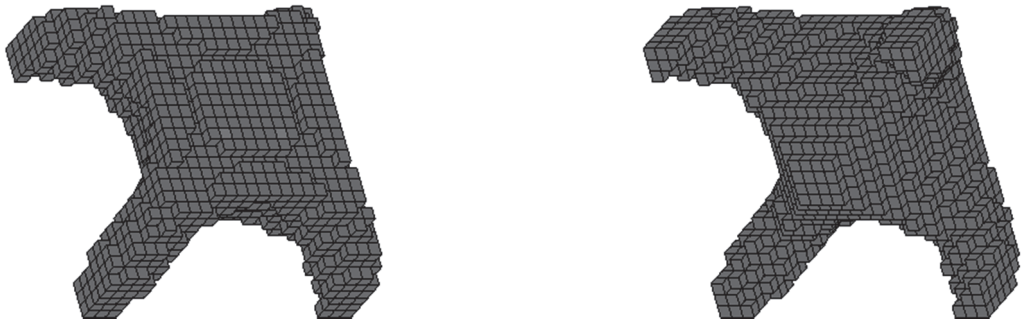

(c) Freeform result (compliance = 14.40)

Fig. 14 Topology optimization results of the cube structure problem

From the results, the following conclusions can be drawn:

(1) The hybrid result shown in Fig. 14a is only a local optimum because it obviously can be further optimized.

(2) By reducing the L_{lim} value, the hybrid result shown in Fig. 14b yields much better structural performance as compared to Fig. 14a.

(3) Optimality of the hybrid result in Fig. 14b is compatible to that of the freeform result shown in Fig. 14c. Therefore, the new topology optimization method is practically meaningful by concurrently addressing the design manufacturability and optimality.

7.2 Cantilever structure problem

Figure 15a demonstrates the initial design domain (10*50*26) and the attached boundary conditions of the cantilever structure problem. A force of magnitude 2 is loaded and the dark blue color represents the fixed elements. In addition, a symmetric surface (shown in green) is added in order to save the computational resource and thus, only half of the cantilever is demonstrated. The solid material employs a Young's modulus value of 1 and Poison's ratio value of 0.3. The optimization problem is to minimize the structural compliance under the maximum material volume ratio of 0.5.

For the full cantilever, the front and back surfaces are shape preserved while the others are freeform. It is assumed that the cutter axis is perpendicular to the front and back surfaces and hence, the front machining feature candidate demonstrated in Fig. 15b is adopted.

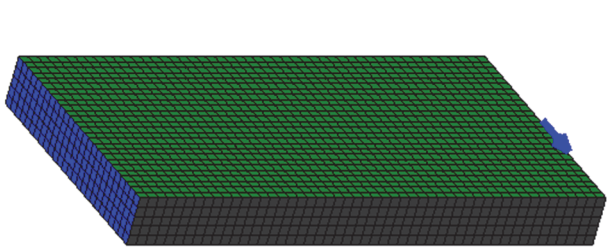

(a) Boundary condition in the front view

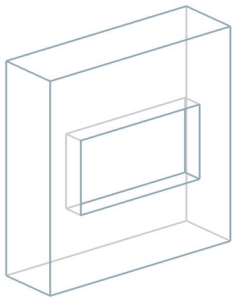

(b) Front machining feature candidate

Fig. 15 Problem setup for the 3D cantilever structure

Again, two schemes will be explored in this example with the threshold value L_{lim} equal to 50*26 and 0.5*50*15, respectively. Correspondingly, the optimization results are plotted in Fig. 16.

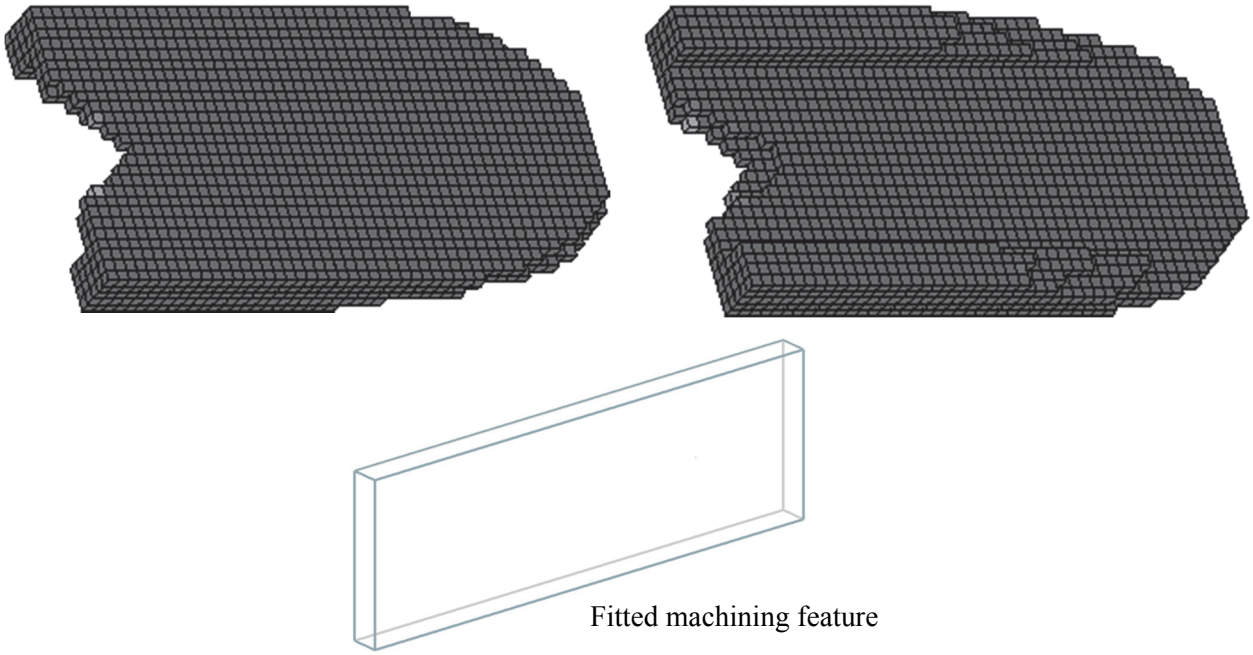

Fitted machining feature

(a) Result with $L_{lim} = 24 * 15$ (compliance = 52.96)

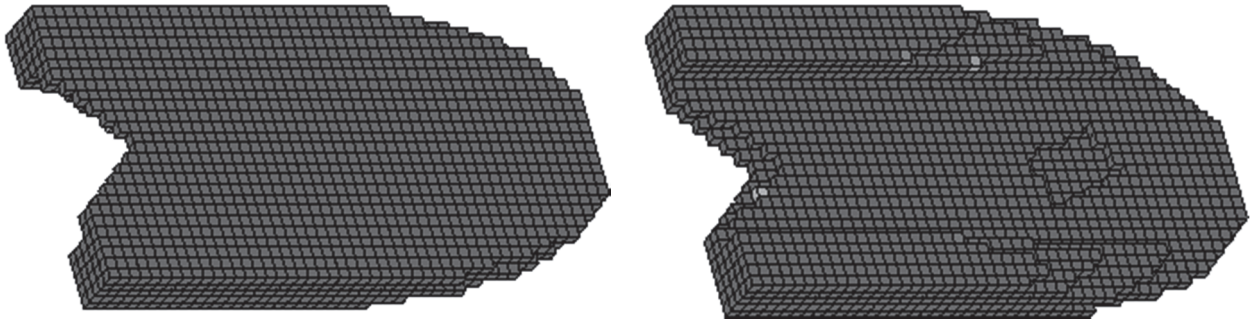

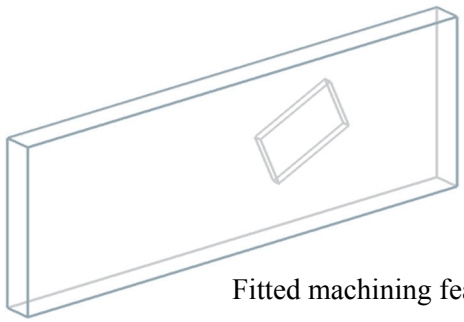

(b) Result with $L_{lim} = 0.5 * 24 * 15$ (compliance = 52.55)

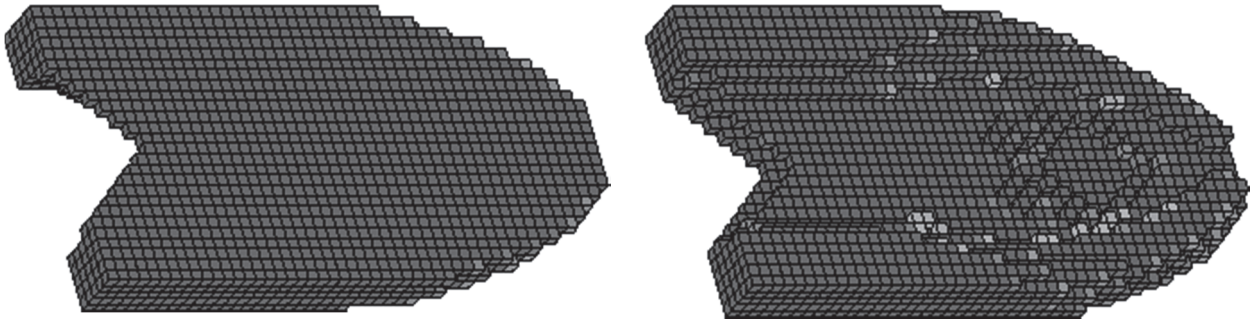

(c) Freeform result (compliance = 52.25)

Fig. 16 Topology optimization results of the cantilever structure problem

By analyzing the optimization results, similar conclusions can be drawn as compared to the last example.

7.3 A Multi-direction 2.5D machining example

In this sub-section, a multi-direction 2.5D machining example will be studied. Here, the multi-direction means spatial relationship between the part and the cutter axis is not unique. As shown in Fig. 17a, faces 1 and 2 employ the cutter axis in *x*-axis direction and faces 2 and 4 have the cutter axis in *z*-axis direction. Therefore, all faces 1-4 are shape preserved and will be fitted with the front machining feature. The candidate is plotted in Fig. 17b. In order to enhance the design freedom, this slot feature has its sectional nodal positions as the variables for the least squares fitting problem, which could derive the sectional shape of an arbitrary quadrangle. In addition, the rib is non-designable and all other surfaces are freeform.

Figure 17a presents the initial design domain (25*40*25) and the corresponding boundary conditions. A force of magnitude 0.01 is loaded on top of the design and the two through-holes at the bottom plate are fixed. The solid material employs a Young's modulus value of 1 and Poison ratio value of 0.3. The optimization problem is to minimize the structural compliance under the maximum material volume ratio of 0.4.

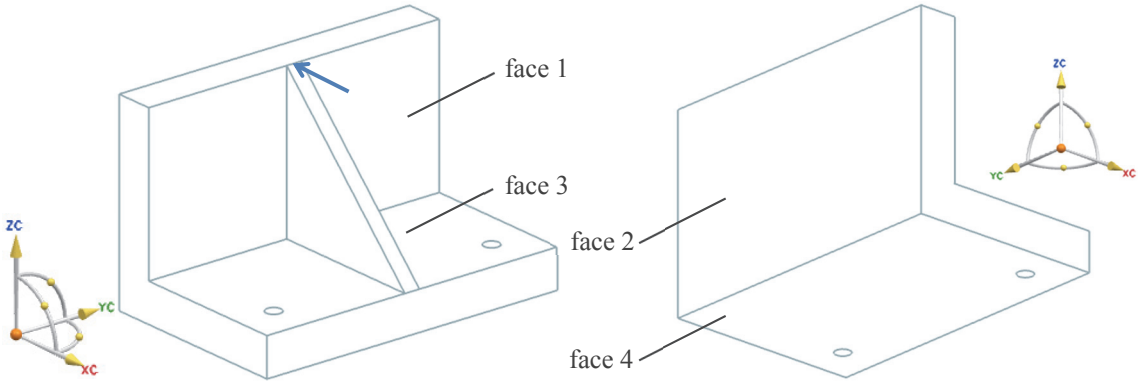

(a) Initial design domain and boundary condition

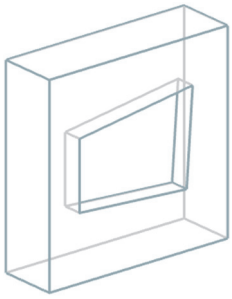

(b) Front machining feature candidate

Fig. 17 Problem setup

The threshold value L_{lim} is 40*20 and the optimization results are demonstrated in Fig. 18.

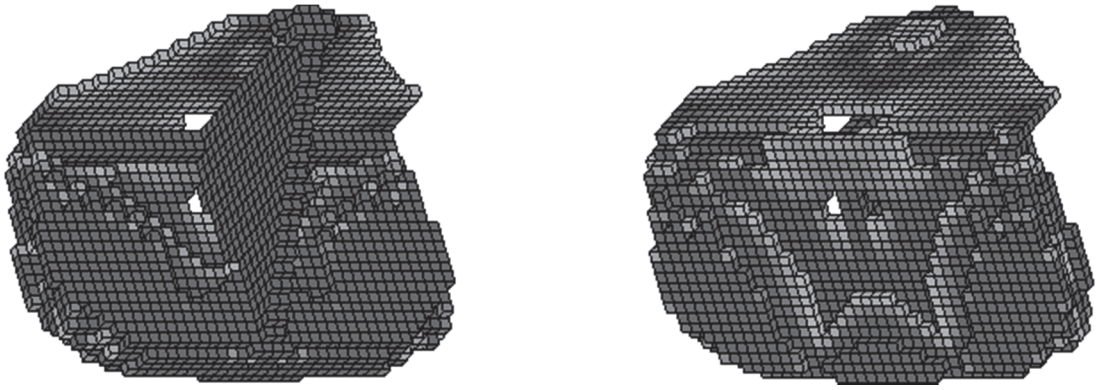

(a) Freeform result (compliance = 2.45)

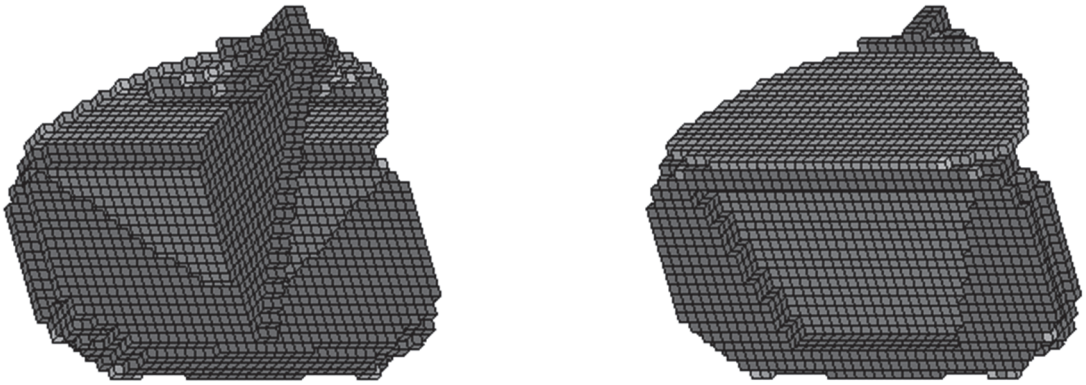

(b) Result for hybrid manufacturing (compliance = 2.70)

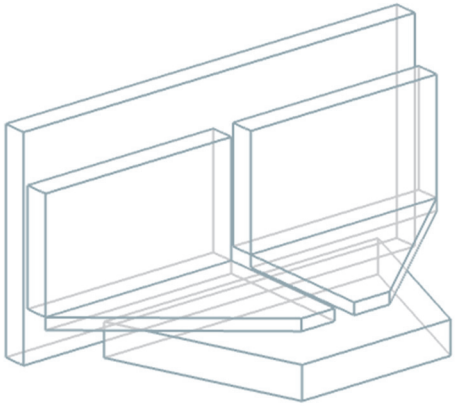

(c) Removed machining features

Fig. 18 Topology optimization results for the bracket problem

In this example, the machining features have been successfully generated through multiple directions and the overall material distributions are similar between the hybrid result (see Fig. 18b) and the freeform result (see Fig. 18a). However, sacrifice of the result optimality is bigger than that of the last two examples. For this reason, the feature fitting result is dependent on the input feature parameters and could be trapped at a local optimum. Solution for this problem is currently under active exploration.

7.4 A compound machining example

Compound machining feature generally can be divided into two categories, as demonstrated in Fig. 19. For the compound feature type 1, it can be realized through the multi-time feature fittings which were earlier conducted in Sections 7.1 and 7.2. Therefore, this section will explore the realization of the compound feature type 2. The strategy is to divide the initial design domain into multiple sub-domains and each of them will be subject to independent feature fitting. Division of the initial design domain requires user input, which is a reflection of the design intent.

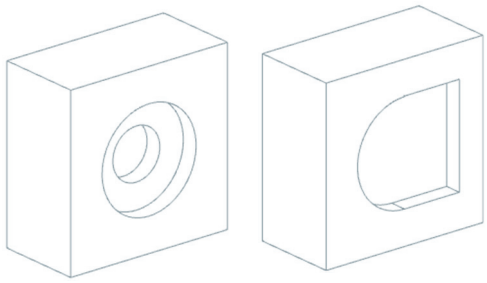

(a) Compound feature type 1 (b) Compound feature type 2

Fig. 19 Compound machining features

The example studied in this sub-section is an L-shape torque arm (10*50*50), as plotted in Fig. 20. The initial design domain is divided into four sub-domains: The two cylindrical areas belong to non-designable sub-domains, where the force is loaded at the top one and the fixed boundary condition is applied to the bottom one. The torque arm body is divided into two sub-domains by the reference plane which will be treated as disconnected when performing feature fitting.

As demonstrated in Fig. 20, the grey-color surface in the front view is shape preserved while the grey-color surface in the back view is freeform. The other surfaces of the torque arm body are non-designable. The feature candidate presented in Fig. 17b is re-applied. The solid material employs a Young's modulus value of 1 and Poison ratio value of 0.3. The optimization problem is to minimize the structural compliance under the maximum material volume ratio of 0.6.

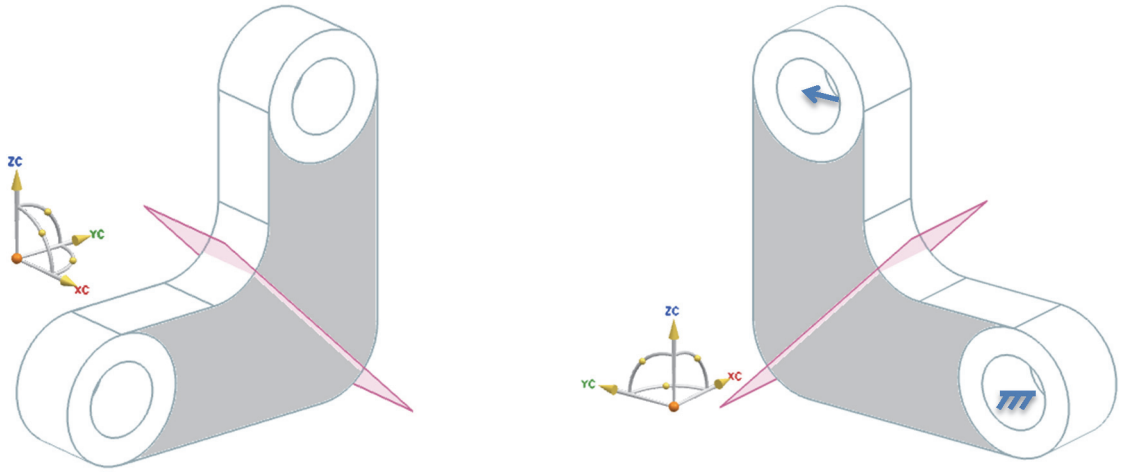

(a) Front view (b) Back view

Fig. 20 The L-shape torque arm

The threshold value L_{lim} is 30*20 and the optimization results are demonstrated in Fig. 21.

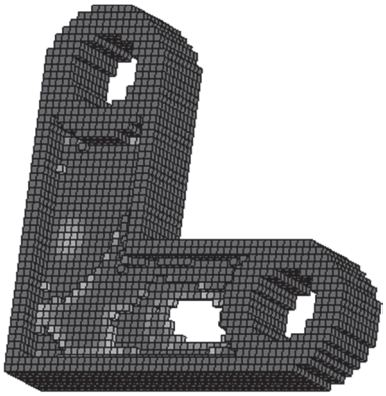

(a) Freeform result in back view (compliance = 5.35)

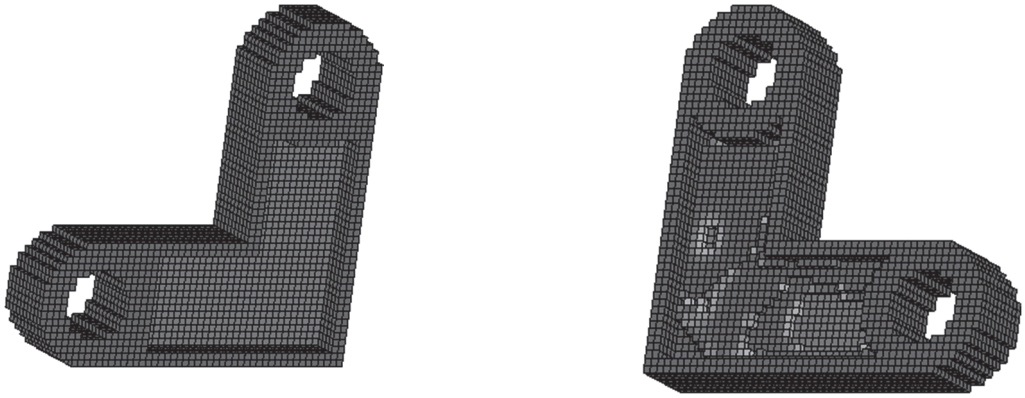

(b) Result for hybrid manufacturing (compliance = 5.43)

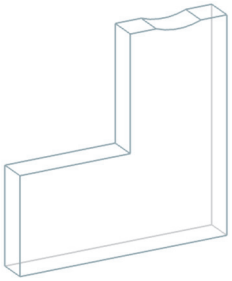

(c) Removed machining features

Fig. 21 Topology optimization results for the L-shape torque arm

In this example, the compound feature type 2 is successfully generated through the domain division and the derived hybrid result is compatible in structural performance to the freeform result. Currently, an automated domain division algorithm is under exploration which would facilitate the topology optimization model preparation.

7.5 A discussion about the convergence issue

As mentioned earlier, there are convergence issues for the proposed topology optimization method because of the repeatedly performed least squares fitting. It is difficult for the objective function to reach a stable value. Hence, two approaches can be applied to fix this convergence issue: (1) Using fixed

iteration number or (2) stabilizing the objective function value of the feature based result. The former is easy to understand but only an optimized result is derived. Therefore, the latter is employed in this work, through which the optimization process converges in case that the feature based result is no longer being modified.

To be specific, convergence histories of the cube design in Fig. 14b, the cantilever design in Fig. 16b, and the bracket design in Fig. 18b are demonstrated in Fig. 22. We can see from the histories that, even though oscillations are always there, objective values of the feature-based results finally stabilize, which indicates there is no more room for further improvement. It is noted that, the red curves approximate the convergence histories of the feature based results subject to N=15.

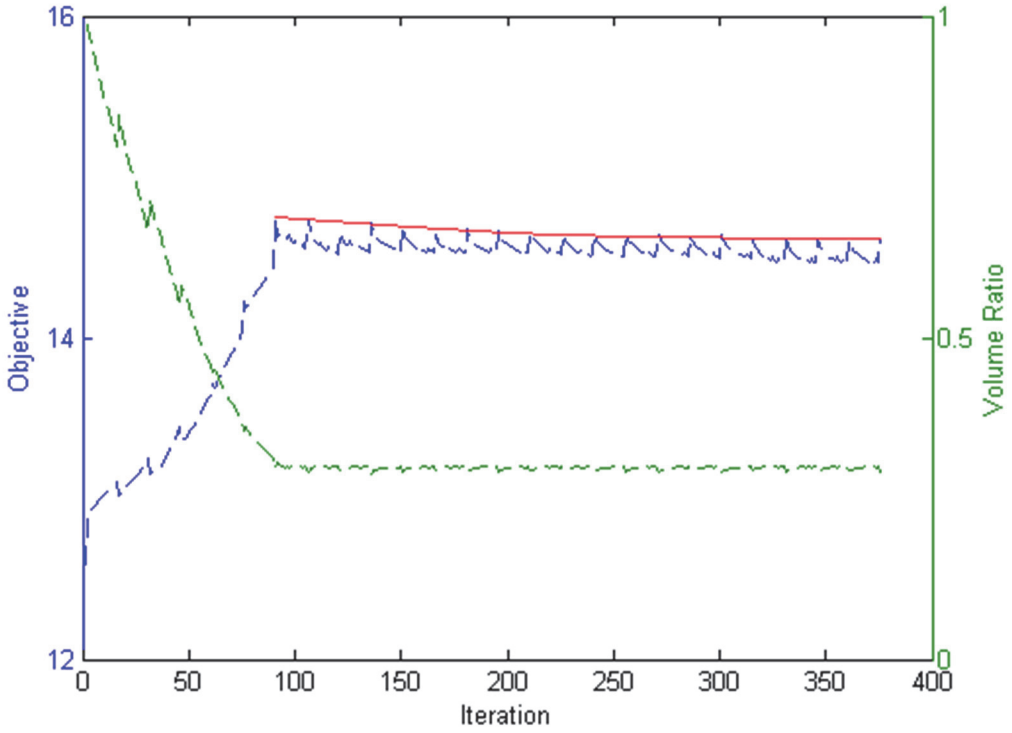

(a) The cube design in Fig. 14b

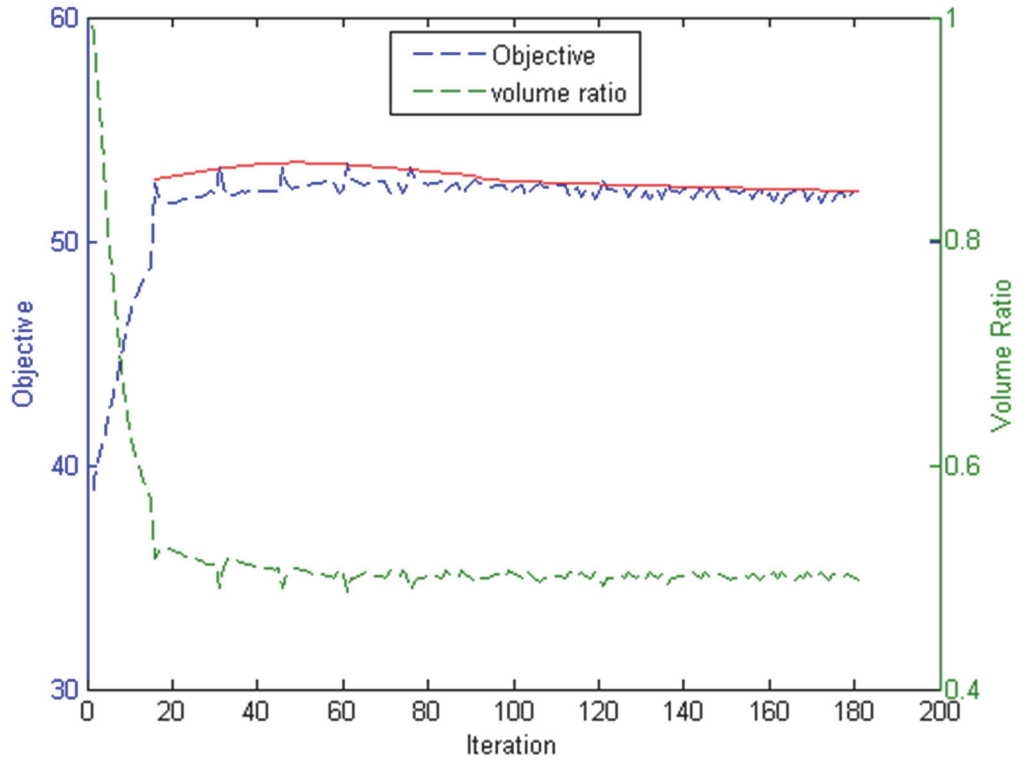

(b) The cantilever design in Fig. 16b

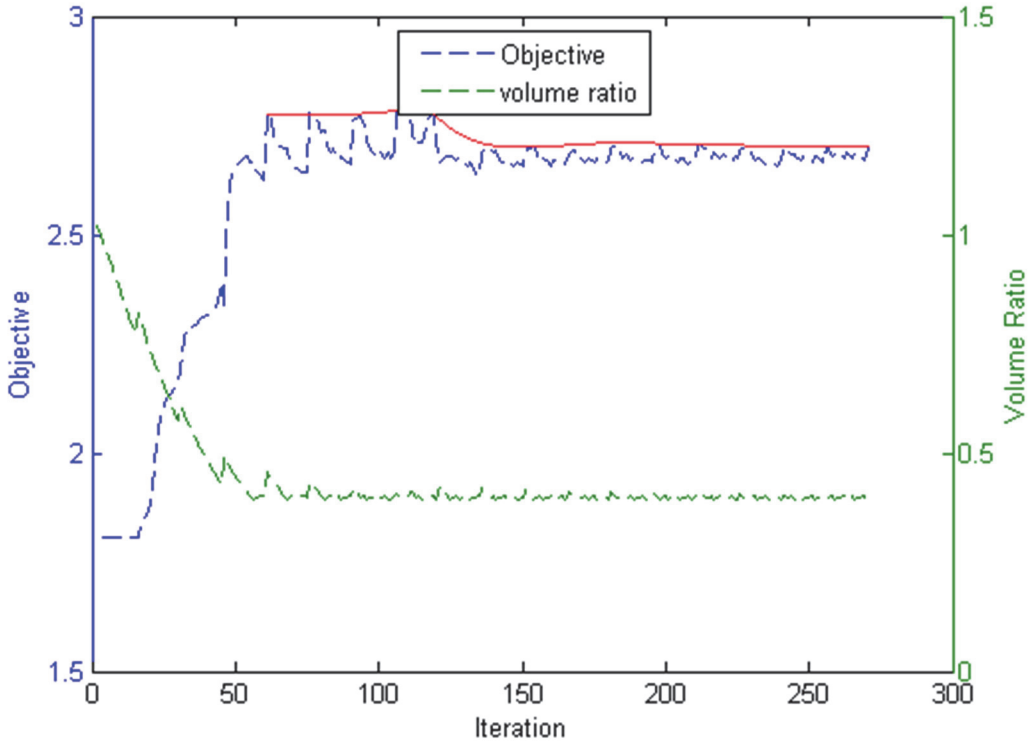

(c) The bracket design in Fig. 18b

Fig. 22 Convergence histories

8. Conclusion

This paper presents a topology optimization method for hybrid additive-subtractive manufacturing, which has been successfully implemented by designing a few 3D structures. Some key findings can be drawn from the numerical examples that:

(1) The derived hybrid design, at most times, demonstrates compatible structural performance compared to the traditional 3D freeform result.

(2) The method can cover a wide range of 2.5D machining features, including the front and side machining features, and the compound machining features. In addition, the multi-direction 2.5D machining can also be addressed by the proposed method.

(3) Result optimality of the hybrid design is strongly dependent on the layers of feature fitting. More layers generally yield more optimal result, even though the manufacturability will be reduced.

From another perspective, the topology optimization method for hybrid design proposed in this paper is developed based on the casting-SIMP [Gersborg and Andreasen 2011], which was proposed to address the no-undercut issue for injection molding/casting parts. The purpose of employing the casting-SIMP for 3D printing part optimization is to create the clearly identified structural boundary and enable the structural boundary-based propagation. In this way, part of the boundaries can be fitted with machining features to facilitate the post-machining. At the same time, the casting-SIMP produces the no-undercut design which improves the least squares fitting accuracy, because undercuts generally do not appear in machining feature definitions for being non-manufacturable. Another major difference compared to the conventional casting-SIMP is that the multi-axis based material removal/addition is enabled; instead of only along a fixed draw direction.

The proposed topology optimization method has been developed and implemented using structured finite element mesh. The method is currently being extended to employ unstructured mesh and its formulation and performance will be reported in the future.

Acknowledgement

The authors would like to acknowledge the support from China Scholarship Council (CSC) and National Science Foundation.

Reference

Allaire G, Jouve F, Toader AM (2004) Structural optimization using sensitivity analysis and a level-set method. J. Comput. Phys. 194:363–393

Allaire G, Jouve F, Michailidis G (2013) Casting constraints in structural optimization via a level-set method. *10th World Congress on Structural and Multidisciplinary Optimization*, Orlando, Florida, USA

Allaire G, Jouve F, Michailidis G (2016) Thickness control in structural optimization via a level set method. Struct. Multidisc. Optim. 53:1349-4382

Bendsoe MP, Sigmund O (2004) Topology optimization: theory, methods and applications, 2nd edition, Springer, Berlin

Bracket D, Ashcroft I, Hague R (2011) Topology optimization for additive manufacturing. 22nd Annual International Solid Freeform Fabrication Symposium, Austin, TX

Chen JQ, Shapiro V, Suresh K, Tsukanov I (2007) Shape optimization with topological changes and parametric control. Int. J. Numer. Methods Eng. 71:313-346

Chen JQ, Freytag M, Shapiro V (2008a) Shape sensitivity of constructively represented geometric models. Comput. Aided Geom. Des. 25:470-488

Chen SK, Wang MY, Liu AQ (2008b) Shape feature control in structural topology optimization. Comput. Aided Des. 40:951-962

Cheng GD, Mei YL, Wang XM (2006) A feature-based structural topology optimization method. IUTAM Symposium on Topological Design Optimization of Structures, Machines and Materials, 505-514

Deaton JD, Grandhi RV (2014) A survey of structural and multidisciplinary continuum topology optimization: post 2000. Struct. Multidisc. Optim. 49:1-38

Eschenauer HA, Olhoff N (2001) Topology optimization of continuum structures: A review. Appl. Mech. Rev. 54:331:390

Flynn JM, Shokrani A, Newman ST, Dhokia V (2016) Hybrid additive and subtractive machine tools – Research and industrial developments. Int. J. Mach. Tools Manuf. 101:79-101

Gao HH, Zhu JH, Zhang WH, Zhou Y (2015) An improved adaptive constraint aggregation for integrated layout and topology optimization. Comput. Methods Appl. Mech. Eng. 289:387-408

Gaynor AT, Meisel NA, Williams CB, Guest JK (2014) Multiple-material topology optimization of compliant mechanisms created via PolyJet three-dimensional printing. J. Manuf. Sci. Eng. 136:061015

Garden N, Schneider A (2015) Topological optimization of internal patterns and support in additive manufacturing. J. Manuf. Syst. 37:417-425

Gersborg AR, Andreasen CS (2011) An explicit parameterization for casting constraints in gradient driven topology optimization. Struct. Multidisc. Optim. 44:875-881

Gopalakrishnan SH, Suresh K (2008) Feature sensitivity: A generalization of topological sensitivity. Finite Elem. Anal. Des. 44:696-704

Guest JK, Prevost JH, Belytschko T (2004) Achieving minimum length scale in topology optimization using nodal design variables and projection functions. Int. J. Numer. Methods Eng. 61:238-254

Guest JK (2009a) Topology optimization with multiple phase projection. Comput. Methods Appl. Mech. Eng. 199:123-135

Guest JK (2009b) Imposing maximum length scale in topology optimization. Struct. Multidisc. Optim. 37:463-473

Guest JK, Zhu M (2012) Casting and milling restrictions in topology optimization via projection-based algorithms. *Proceedings of the ASME 2012 International Design Engineering Technical Conference & Computers and Information in Engineering Conference*, Chicago, IL, USA

Guest JK (2015) Optimizing the layout of discrete objects in structures and materials: A projection-based topology optimization approach. Comput. Methods Appl. Mech. Eng. 283:330-351

Guo X, Zhang WS, Zhong WL (2014a) Explicit feature control in structural topology optimization via level set method. Comput. Methods Appl. Mech. Eng. 272:354-378

Guo X, Zhang WS, Zhong WL (2014b) Doing topology optimization explicitly and geometrically – A new moving morphable components based framework. J. Appl. Mech. 81:081009-1:12

Ha SH, Guest JK (2014) Optimizing inclusion shapes and patterns in periodic materials using Discrete Object Projection. Struct. Multidiscip. Optim. 50:65–80

Hoque ASM, Halder PK, Parvez MS, Szecsi T (2013) Integrated manufacturing features and Design-for-manufacture guidelines for reducing product cost under CAD/CAM environment. Comput. Ind. Eng. 66:988-1003

Kang Z, Wang YQ (2013) Integrated topology optimization with embedded movable holes based on combined description by material density and level sets. Comput. Methods Appl. Mech. Eng. 255:1-13

Kang M, Kim G, Eum K, Park MW, Kim JK (2014) A classification of multi-axis features based on manufacturing process. Int. J. Precis. Eng. Manuf. 15:1255-1263

Kang Z, Wang YG, Wang YQ (2016) Structural topology optimization with minimum distance control of multiphase embedded components by level set method. Comput. Methods Appl. Mech. Eng. 306:299-318.

Khanoki SA, Pasini D (2012) Multiscale design and multiobjective optimization of orthopedic hip implants with functionally graded cellular material. J. Biomech. Eng. 134:031004

Lauwers B, Klocke F, Klink A, Tekkaya AE, Neugebauer R, Mcintosh D (2014) Hybrid processes in manufacturing. CIRP Ann. Manuf. Technol. 63:561-583

Lazarov BS, Wang FW, Sigmund O (2016) Length scale and manufacturability in density-based topology optimization. Arch. Appl. Mech. 86:189-218

Leary M, Merli L, Torti F, Mazur M, Brandt M (2014) Optimal topology for additive manufacture: A method for enabling additive manufacture of support-free optimal structures. Mater. Des. 63:678-690.

Liu JK, Ma YS (2015) 3D level-set topology optimization: a machining feature-based approach. Struct. Multidisc. Optim. 52:563-582

Liu JK, Ma YS, Fu JY, Duke K (2015a) A novel CACD/CAD/CAE integrated design framework for fiber-reinforced plastic parts. Adv. Eng. Softw. 87:13-29

Liu JK (2016) Guidelines for AM part consolidation, Virtual Phys. Prototyp. 11:133-141.

Liu ST, Li Q, Chen WJ, Hu R, Tong LY (2015b) H-DGTP – a Heaviside-function based directional growth topology parameterization for design optimization of stiffener layout and height of thin-walled structures. Struct. Multidisc. Optim. 52:903-913

Lu JN, Chen YH (2012) Manufacturable mechanical part design with constrained topology optimization. J. Eng. Manuf. 226:1727-1735

Luo JZ, Luo Z, Chen SK, Tong LY, Wang MY (2008) A new level set method for systematic design of hinge-free compliant mechanisms. Comput. Methods Appl. Mech. Eng. 198:318-331

Masmiati N, Sarhan AAD, Hamdi M (2012) Optimizing the cutting parameters for better surface quality in 2.5D cutting utilizing titanium coated carbide ball end mill. Int. J. Precis. Eng. Manuf. 13:2097-2102

Meisel N, Williams C (2015) An investigation of key design for additive manufacturing constraints in multimaterial three-dimensional printing. J. Mech. Des. 137:111406

Mei YL, Wang XM, Cheng GD (2008) A feature-based topological optimization for structure design. Adv. Eng. Softw. 39:71-87

Munk DJ, Vio GA, Steven GP (2015) Topology optimization methods using evolutionary algorithms: a review. Struct. Multidisc. Optim. doi: 10.1007/s00158-015-1261-9

Norato JA, Bell BK, Tortorelli DA (2015) A geometry projection method for continuum-based topology optimization with discrete elements. Comput. Methods Appl. Mech. Eng. 293:306-327

Poulsen TA (2003) A new scheme for imposing a minimum length scale in topology optimization. Int. J. Numer. Methods Eng. 57:741-760

Rozvany GIN (2001) Aims, scope, methods, history and unified terminology of computer-aided topology optimization in structural mechanics. Struct. Multidisc. Optim. 21:90-108

Rozvany GIN (2009) A critical review of established methods of structural topology optimization. Struct. Multidisc. Optim. 37:217-237

Schevenels M, Lazarov BS, Sigmund O (2011) Robust topology optimization accounting for spatially varying manufacturing errors. Comput. Methods Appl. Mech. Eng. 200:3613-3627

Schramm U, Zhou M (2006) Recent developments in the commercial implementation of topology optimization. In: IUTAM symposium on topological design optimization of structures, machines and materials, Springer, vol.137, pp:239-248

Sigmund O (2007) Morphology-based black and white filters for topology optimization. Struct. Multidisc. Optim. 33:401-424

Sigmund O (2009) Manufacturing tolerant topology optimization. Acta Mech. Sin. 25:277-239

Sigmund O, Maute K (2013) Topology optimization approaches. Struct. Multidisc. Optim. 48:1031-1055

Stromberg N (2010) Topology optimization of structures with manufacturing and unilateral contact constraints by minimizing an adjustable compliance-volume product. Struct. Multidisc. Optim. 42:341-350

Tang YL, Kurtz A, Zhao YF (2015) Bidirectional evolutionary structural optimization (BESO) based design method for lattice structure to be fabricated by additive manufacturing. Comput. Aided Des. 69:91-101

Ulu E, Korkmaz E, Yay K, Ozdoganlar OB, Kara LB (2015) Enhancing the structural performance of additively manufactured objects through build orientation optimization. J. Mech. Des. 137:111410

van Dijk NP, Maute K, Langelaar M, van Keulen F (2013) Level-set methods for structural topology optimization: a review. Struct. Multidisc. Optim. 48:437-472

Verma AK, Rajotia S (2008) A hint-based machining feature recognition system for 2.5D parts. Int. J. Prod. Res. 46:1515-1537

Wang FW, Lazarov BS, Sigmund O (2011) On projection methods, convergence and robust formulations in topology optimization. Struct. Multidisc. Optim. 43:767-784

Wang MY, Wang XM, Guo DM (2003) A level set method for structural topology optimization. Comput. Methods Appl. Mech. Eng. 192:227–246

Wang YQ, Zhang L, Wang MY (2016) Length scale control for structural optimization by level sets. Comput. Methods Appl. Mech. Eng. 305:891-909

Xia L, Zhu JH, Zhang WH, Breitkopf P (2013) An implicit model for the integrated optimization of component layout and structure topology. Comput. Methods Appl. Mech. Eng. 257:87-102

Xia Q, Shi TL, Wang MY, Liu SY (2010) A level set based method for the optimization of cast part. Struct. Multidisc. Optim. 41:735-747

Xia Q, Shi TL (2015) Constraints of distance from boundary to skeleton: For the control of length scale in level set based structural topology optimization. Comput. Methods Appl. Mech. Eng. 295:525-542

Xie YM, Steven GP (1993) A simple evolutionary procedure for structural optimization. Comput. Struct. 49: 885-896

Xu JT, Sun YW, Zhang XK (2013) A mapping-based spiral cutting strategy for pocket machining. Int. J. Adv. Manuf. Technol. 67:2489-2500

Zegard T, Paulino GH (2015) Bridging topology optimization and additive manufacturing. Struct. Multidisc. Optim. DOI: 10.1007/s00158-015-1274-4

Zhang WH, Xia L, Zhu JH, Zhang Q (2011) Some recent advances in the integrated layout design of multicomponent systems. J. Mech. Des. 133:104503-1-15

Zhang J, Zhang WH, Zhu JH, Xia L (2012) Integrated layout design of multi-component systems using XFEM and analytical sensitivity analysis. Comput. Methods Appl. Mech. Eng. 245-246:75-89

Zhang WS, Zhong WL, Guo X (2014) An explicit length scale control in SIMP-based topology optimization. Comput. Methods Appl. Mech. Eng. 282:71-86

Zhang WS, Zhong WL, Guo X (2015a) Explicit layout control in optimal design of structural systems with multiple embedding components. Comput. Methods Appl. Mech. Eng. 290:290-313

Zhang WS, Yuan J, Zhang J, Guo X (2016) A new topology optimization approach based on Moving Morphable Components (MMC) and the ersatz material model. Struct. Multidisc. Optim. 53:1243-1260

Zhang P, Toman J, Yu YQ, Biyikli E, Kirca M, Chmielus M, To AC (2015b) Efficient design-optimization of variable-density hexagonal cellular structure by additive manufacturing: theory and validation. J. Manuf. Sci. Eng. 137:021004.

Zhou M, Fleury R, Shyy YK, Thomas HL (2002) Progress in topology optimization with manufacturing constratins. Proceedings of 9th AIAA/ISSMO symposium on multidisciplinary analysis and optimization , Atlanta, GA, USA

Zhou MD, Wang MY (2013) Engineering feature design for level set based structural optimization. Comput. Aided Des. 45:1524-1537

Zhou MD, Lazarov BS, Wang FW, Sigmund O (2015) Minimum length scale in topology optimization by geometric constraints. Comput. Methods Appl. Mech. Eng. 293:266-282

Zhu JH, Gao HH, Zhang WH, Zhou Y (2015) A multi-point constraints based integrated layout and topology optimization design for multi-component systems. Struct. Multidisc. Optim. 51:397-407

Zhu Z, Dhokia V, Nassehi A, Newman ST (2013) A review of hybrid manufacturing processes – state of the art and future perspectives. Int. J. Comput. Integr. Manuf. 26:596-615